Amorphous molybdenum sulphide @ nanoporous gold as catalyst for hydrogen evolution reaction in acidic environment

Amorphous Molybdenum Sulphide @ Nanoporous Gold as Catalyst for Hydrogen Evolution Reaction in Acidic Environment

F. Scaglione[1*], Y. Xue[1], F. Celegato[2], P. Rizzi[1], L. Battezzati[1]

[1]Dipartimento di Chimica and Centro Interdipartimentale NIS (Nanostructured Interfaces and Surfaces), Università di Torino, V. Giuria 7, 10125 Torino, Italy.
[2]Istituto Nazionale di Ricerca Metrologica (INRIM), Str. delle Cacce, 91, 10135 Torino, Italy

Federico Scaglione (*corresponding author), Ph.D., federico.scaglione@unito.it
Yanpeng Xue, Ph.D.,
Federica Celegato, Bachelor of Science,
Paola Rizzi, Professor,
Livio Battezzati, Professor.

Abstract

A novel catalyst for water splitting has been prepared by Linear Sweep Voltammetry (LSV) deposition of amorphous MoS_2 on nanoporous gold (NPG) obtained by electrochemical de-alloying a metallic glass precursor, $Au_{40}Cu_{28}Ag_7Pd_5Si_{20}$ (at.%). As a function of number of CV cycles, Au ligaments are progressively encapsulated by a thin layer of amorphous MoS_2 catalyst for hydrogen evolution. NPG provides a good substrate for deposition having excellent properties of handability and mechanical resistance in addition to catalytic activity, high conductivity and high surface area. By controlling the number of cycles in LSV low onset potential, low Tafel slope and interesting values of exchange current density were obtained. The synergistic behaviour of the multi-component material provides an highly efficient catalyst for hydrogen making of these samples a good candidate in some instances comparable to the conventional Pt catalyst for hydrogen evolution in acidic environment.

Keywords: De-alloying, nanoporous gold, MoS_2, hydrogen evolution reaction, electrodeposition.

1. Introduction

The challenge of reducing CO_2 emissions responsible for global warming while coping with an ever-increasing global demand for energy implies the substitution of conventional fossil fuels with green and renewable sources [1,2]. Hydrogen is a promising high energy-density fuel [3,4], however, molecular hydrogen is not available in nature and must be extracted from the most abundant molecule in nature, i.e. water [5]. Electrochemical water splitting into molecular hydrogen and oxygen requires a large overpotential that can be reduced by using catalysts [6]. Among these, Pt is the most active for hydrogen evolution reaction (HER); on the other hand, it is highly expensive and of limited availability in nature [7]. Efforts to find a substitute for Pt with comparable catalytic activity have prompted in recent years studies on non-precious-metal catalyst [8], among which molybdenum dichalcogenides (MoS_2, $MoSe_2$) have provided promising results [9].

This family of semiconducting materials finds manifold uses because of their intrinsic properties: the bandgap matches well the solar spectrum for application in solar cells [10] and rechargeable batteries [11]; the layer-type structure composed of intercalated molybdenum and sulphur monolayers, is well suited as solid lubricant [12]; catalytic properties are exploited in heterogeneous catalysis for hydrodesulphurization of petroleum [13] and for hydrogen evolution reaction (HER) [14].

Several methods have been reported in the literature for preparing MoS_2: mechanical and solution exfoliation [15,16]; chemical and physical vapour deposition [17,18]; hydrothermal synthesis [19,20]; sulfurization of molybdenum oxides [21]. These techniques are time consuming and cost intensive whereas electrochemical deposition [14,22,23] is attractive after setting properly growth parameters such as applied potential, current, temperature and pH of the bath, in that it requires a relatively cheap equipment and is generally fast [24]. The most promising reaction is the cathodic reduction of ammonium or sodium tetrathiomolybdate in aqueous solution [14]. This method requires as substrate an electrode with excellent conductive properties, mechanical stability and high surface area.

Nanoporous metals obtained by selective removal of less noble elements from an alloy fit these substrates requirements; among them, nanoporous gold (NPG) can be prepared by de-alloying Au alloys (e.g. Ag-Au, Cu-Au, complex Au-based amorphous alloys)[25,26,27] or by anodic roughening Au films [28, 29]. De-alloyed NPG is made of interconnected pores and ligaments whose morphology depends on the crystalline or amorphous state of the master alloy [30]. In fact, by de-alloying crystalline alloys, the starting microstructure is retained and each grain evolves in a porous single crystal [31], contrary to the case of metallic glass precursors from which numerous

fine crystals are produced and ligaments result from their impingement [32, 33]. In both cases, the surface diffusion of the remaining noble atoms is the driving mechanism for ligament formation. Since a complex composition is mandatory for glass forming ability, less noble atoms (e.g, Ag, Pd for Au-based glasses) are incorporated as impurity in the newly formed crystals and ligaments [34]. Finally, the most common technique for the production of amorphous alloys, i.e. melt spinning, gives thin ribbons which are free-standing. This shape is maintained after de-alloying and helps in handling for further processes.

The idea to combine the peculiar properties of nanoporous gold, i.e. free standing samples, mechanical resistance, high surface area and high catalytic activity, with the well known catalytic properties of MoS_2 was already explored recently. NPG prepared by free corrosion of a Ag-Au alloy was covered with a thin layer of amorphous molybdenum sulphide grown on the internal surface of pores by chemical plating reaction between a precursor and hydrazine as reducer. This catalyst resulted efficient for HER [35].

In this paper the NPG obtained from free corrosion of crystalline Ag-Au has been replaced with NPG from an amorphous precursor. This NPG substrate exhibits superior catalytic activity due to the morphology of ligaments: while ligaments of NPG prepared from dealloying crystalline alloys are smooth and constituted by a single crystal, NPG from an amorphous precursor is composed of defective impinged nano-sized crystals with incorporated impurities of Ag and Pd atoms which may provide further active sites for reactions [34]. Moreover, a different method of deposition of molybdenum sulphide was chosen, i.e. CV cycling in aqueous solution at room temperature, a fast technique and safer for the operator.

2. Experimental Details

General. A $Au_{40}Cu_{28}Ag_7Pd_5Si_{20}$ master alloy was prepared by arc-melting lumps of pure elements in Ti-gettered Ar atmosphere. Amorphous ribbons, 25 μm thick and 2 mm wide, were prepared by melt-spinning the master alloy at a linear speed of 25 m s^{-1} onto a copper wheel in a closed chamber kept under Ar protective atmosphere. Samples 20 mm in length were cut for de-alloying.

De-alloying of the as-spun ribbons have been performed in 1 M H_2SO_4 aqueous solution in a three electrode cell (saturated Ag/AgCl double bridge reference electrode, Pt counter-electrode, the sample as working electrode). From previous works [32,33], the de-alloying potential was set at 1.05 V at the temperature of 70 °C to increase the rate of dissolution and achieve a complete de-alloying through the whole thickness of the ribbon in 6 h. After de-alloying ribbons are easy-to-

handle and free standing, therefore they can be used as electrodes for the further step of MoS_2 electrochemical deposition carried out by CV technique using the three-electrode cell mentioned above. In this case, to get an homogeneous deposition, a Pt cylindrical grid has been used as counter electrode, putting the de-alloyed sample in the middle as working electrode. The electrolyte had volume of 250 ml 0.005 M Na_2MoS_4 solution, kept under mild stirring condition inside a closed cell. Solution was freshly prepared from chemical grade reagents and Milli-Q deionised water (18.2 MΩ) and was purged with N_2 for 1 hour before experiment. Four samples have been prepared increasing the number of CV scan of 5, 10, 25 and 50 and are designated 5CV@NPG, 10CV@NPG, 25CV@NPG, 50CV@ NPG, respectively.

Characterization. The structure and microstructure of samples was studied, before and after etching and after MoS_2 electrodeposition, by X-ray diffraction (XRD) in Bragg-Brentano geometry with monochromatic Cu-K_α radiation, and Scanning Electron Microscopy (SEM) with Energy Dispersive X-ray Spectroscopy (EDS).

a-MoS_x to c-MoS_2 phase transformation induced by thermal annealing. nCV@NPG (n= 5, 10, 25, 50) samples have been annealed by ramping from RT up to 700 °C under Ar atmosphere and 5 K min^{-1} scan rate in a Diamond DSC.

Raman analyses. Samples, before and after annealing, have been then characterized by Raman analysis performed with a Renishaw inVia Raman Microscope using 514 nm green laser line with an acquisition time of 20 s, 5% power at the sample and a 50 x ULWD objective. The Raman band of silicon wafer at 520 cm^{-1} was used to calibrate the spectrometer.

Hydrogen evolution. The electrocatalytic activity of samples toward HER was evaluated in 0.5 M H_2SO_4 aqueous solution using the same set up of de-alloying experiments; the electrolyte was purged prior to measurements with N_2 for 1 hour. The HER activity was studied by linear sweep voltammetry (LSV) at room temperature for 1000 cycles. A scan speed of 0.5 mVs^{-1} has been chosen for the first ten and every 250^{th} cycles in order to suppress the capacitive current; cycles in between have been performed at higher rate (20 mV s^{-1}) to speed up the experiment. A foil of pure Pt (2x2 cm^2) has been polished on both sides as for conventional metallography and then used as reference in the same experimental conditions. In this work, all current densities have been normalized to the electrochemically active surface area (EASA), while all potentials were referenced to reversible hydrogen electrode (RHE) by adding a value of (0.197 + 0.059 pH)V.

3. Results and Discussion

The formation of NPG by electrochemical de-alloying of $Au_{40}Cu_{28}Ag_7Pd_5Si_{20}$ amorphous precursors has been the subject of a number of previous works describing in details synthesis, morphology and characterization. In summary, this NPG is constituted by ligaments and pores of about 200 nm. Each ligament is composed by several grains impinged on each other during the dealloying of the starting amorphous alloy [36]. The mechanism of dealloying, contrary to crystalline alloys, requires a spontaneous germination step following the irreversible dissolution of less noble elements and surface diffusion of Au adatoms. A multi-grained structure of ligaments results with boundaries emerging on the surface. The fine crystals retain trapped Ag and Pd atoms. The fully de-alloyed ribbon is mechanically stable, and within certain limits, can be bent and handled with tweezers without breaking the sample. Being made up of Au, it has high conductivity while the nanoporous structure gives an extended surface area that is crucial for catalytic applications.

3.1 Electro-deposition of MoS_2

Fully de-alloyed samples of nanoporous gold have been cleaned in concentrated nitric acid and then deeply rinsed in distilled water before treatment. The solution of tetrathiomolybdate ions has been freshly prepared before the experiment by reaction between 5 mM Na_2MoO_4 and excess of Na_2S as follows:

Then HCl has been added while stirring until the pH of 8 was reached and the solution turned dark red because of the formation of thiomolybdate. For electro-deposition by CV the potential has been cycled from -1.6 to 0.1 V (vs Ag/AgCl) at a rate of 50 mV s^{-1}. In **Fig1.** curves obtained at different number of cycles are reported. The current density increases as a function of number of cycles. The surface of samples starts to change colour to dark yellow just after the first cycle and turns black as the surface is covered by a continuous film. Oxidation and reduction signals of deposited moieties [37] appear at -0.15 V and -1 V (vs Ag/AgCl) respectively, well visible in the first scan and then embedded in a broad signal while the current density increases in subsequent

scans. By tuning properly the number of cycles, full coverage of ligaments was achieved avoiding occlusion of pores and formation of a bulk film.

3.2 Microstructure and composition of samples

After de-alloying, NPG is composed of pores and ligaments 200 nm in size measured at their narrower necks. Each ligament is made up of several grains resulting from impingement of crystals independently originated. Grain boundaries are clearly visible in the SEM images of **Fig2a**. EDS analyses of NPG confirms the ligaments are made up of Au with traces of Ag and Pd. In sample 5CV@NPG the morphology of ligaments is still recognized and the presence of a very thin deposited layer has been argued by observing the grain boundaries of impinged crystals, now less visible than in the bare NPG (**Fig2c**). In sample 10CV@NPG ligaments are encapsulated by a coating of MoS_2 which does not reduce the extent of porosity (**Fig2e**). Increasing the number of cycles (i.e. 25CV@NPG), pores are progressively occluded (**Fig2g**), until in sample 50CV@NPG a layer is formed on the top. Breaking this layer discloses the nanoporous material underneath (**Fig 2i**). EDS analyses of samples are reported in Supporting Information **Table S1**. The S/Mo ratio decreases as a function of number of cycles: 3.18, 3.12, 2.68 and 2.08, respectively, after 5, 10, 25 and 50 CV scans. This suggests the composition of molybdenum sulphide around ligaments is close to MoS_3 up to 25 cycles and close to MoS_2 when a continuous layer is formed.

Deposited samples have been annealed under Ar atmosphere up to 700 °C to promote crystallization of a-MoS_x to c-MoS_2. Raman spectra of samples before and after annealing have been performed to proof the amorphous nature of the molybdenum sulphide and are reported in **Fig3**. Before annealing the two broad signals at 450 cm^{-1} and 380 cm^{-1} have been associated to typical vibration $\nu(Mo_3\text{-}\mu S)$ and ν(Mo-S), respectively. They are the characteristic signature of a-MoS_x as a coordination polymer of $[Mo_3S_{13}]^{-2}$ discrete building blocks. After annealing crystallization occurs and the characteristic vibrations of c-MoS_2 appear at 402 cm^{-1} and 380 cm^{-1} [38,39].

As demonstrated in the literature [40], the advantage of having amorphous instead of crystalline MoS_2 is the higher number of under-coordinated surface steps and lattice defects that are created when one layers of MoS_2 deposited on NPG follow the high curvature gradient of gold ligaments. The catalytic activity of MoS_2 catalyst is actually due to under-coordinated atoms and edge sites [9,41].

A further proof of the amorphous nature of the deposited molybdenum sulphide is given by the XRD glazing angle pattern that shows for all samples only reflection of fcc Au in the ribbons, while reflections of molybdenum sulphide have not been detected (**FigS2** in Supporting Information).

3.3 Hydrogen evolution activity of molybdenum sulphide @ NPG

NPG and MoS_2@NPG have been tested for HER by LSV in a 0.5 M H_2SO_4 aqueous solution at room temperature. The sample 50CV@NPG has not been used for catalytic tests because the layer formed on the top of ligaments breaks during the first stages of HER experiments, resulting in an impalpable powder at the bottom of the beaker. All samples exhibit obvious hydrogen evolution activity: in **Fig4** LSV scans have been reported. The current density involved in the process increases as a function of the amount of MoS_2 deposited on ligament. The insets in **Fig4b, 4c** and **4d** show a reduction signal in the first LSV scan, which disappears in the second and following polarization scans. This broad signal is due to the reduction of amorphous MoS_3 to MoS_2 by means of two electrons accepted from to form [14].

Since the electrode is fully stabilized after few LSV cycles, the 10^{th} cycle has been considered to compare the activity of different samples. Then, the stability of the electrodes are compared considering the 1000^{nd} cycle. The catalytic activity towards HER of MoS_2@NPG samples is reported in **Fig5a** and **5d**, together with bare NPG and Pt as references.

The onset potential for HER (**Fig5b**), taken at the point where the current density abruptly increases, has been determined as -178 mV, -106 mV, -136 mV and -109 mV for the bare NPG, 5CV@NPG, 10CV@NPG and 25CV@NPG, respectively, in all cases still far from -29 mV of Pt although the effect of amorphous MoS_2 in decreasing the onset potential is apparent. The major improvement is for sample 5CV@NPG, where the MoS_2 deposition around ligaments is limited, having onset potential reduced of 72 mV with respect to bare NPG.

The stability of the electrodes has been tested for one thousand cycles. In comparison with the curves at the 10^{th} cycle, the current density increases for all samples and the onset of reaction is dramatically shifted close to Pt values: onset of -41 mV, -31 mV, -46 mV and -58 mV have been determined for the bare NPG, 5CV@NPG, 10CV@NPG and 25CV@NPG, respectively (**Fig5e**). These onset values are noticeably lower than those reported for other MoS_2 nanostructures and close to that of Pt (**Table.S2**). To verify reproducibility, HER experiments have been repeated twice with samples prepared in the same manner obtaining comparable results.

Another important criterion for evaluating the catalytic activity of electro-catalysts is the cathodic current density recorded at low applied potential. Values at -0.2 V vs RHE during the 10^{th}

cycle are -35, -18, -19, -6 $\mu A \cdot cm^{-2}$ for bare NPG, 5CV@NPG, 10CV@NPG and 25CV@NPG. An increase is found after the 1000^{th} cycles to -153, -95, -77, -103 $\mu A \cdot cm^{-2}$ for the corresponding samples with an amazing improvement of the current density of 4.4, 5.3, 4.1 and 17.2 time respectively.

The improvement of catalytic activity after long cycling is due to changes in the electrode morphology. In Supporting Information **Table S2**, a comparison of our electrochemical data with different MoS_2 and hybrid materials reported in the literature. In bare NPG ligaments became rougher after cycling (**Fig2b**), with an increase of defects and kink sites for the reaction. Samples 5CV@NPG and 10CV@NPG (**Fig2d and 2f**) show ligaments still covered by MoS_2, as furthermore confirmed by EDS analyses, but more fine grains on the surface are visible, in particular in the former case. In sample 25CV@NPG (**Fig2h**), rearrangement of MoS_2 on the surface has provided coverage of ligaments and a strong reduction of porosity. However the nano-grained layer that was formed provided more active sites to promote the evolution and facilitate the bubbling of molecular hydrogen. As a consequence, the current density increases and the onset of reaction is shifted toward lower values.

3.4 Mechanism of hydrogen evolution

Following the classic theory of hydrogen evolution, the main steps occurring in acidic environment are three: the discharge or Volmer reaction (1), the combination or Tafel reaction (2) and desorption or Heyrovsky reaction (3). A sequence of steps (1) and (2) or (1) and (3), i.e. Volmer- Tafel or Volmer- Heyrovsky, leads to evolution of molecular hydrogen. Below the reactions in details:

(1)

(2)

(3)

where , and are the electron bound in metal, hydrogen atom and molecule adsorbed on metal surface respectively. During Volmer step a transferred electron and a proton react, generating an adsorbed hydrogen atom on the electrode surface. Then, the reaction could proceed either via the Tafel or the Heyrovsky reaction: in the former case, two absorbed

hydrogen atoms combine to generate H_2 whereas in the latter case, another electron reacts with an adsorbed hydrogen atom and another proton from the solution to evolve H_2.

The value of the Tafel slope reflects the rate-determining step (r.d.s.) for the reaction [42,43]. Indeed a slope of 40 mV dec^{-1} indicates that the r.d.s. is a fast discharge reaction (1) and that the coverage of adsorbed hydrogen is less than 10%; a Tafel slope of 60 mV dec^{-1} suggests a large coverage of the surface of adsorbed hydrogen and a combination reaction mechanism (2), while when the r.d.s is the Volmer step (3), a value of 120 mV dec^{-1} arises from various reaction pathways depending on the surface coverage. These values can be used as a guide in determining HER mechanism. Tafel plots of MoS2@NPG are shown for the 10^{th} and 1000^{th} cycles in **Fig5c** and **f** and reported in **Table S2**. Bare NPG gives slope of 160 mV dec^{-1} that decreases to 90 mV dec^{-1} after 1000 cycles, in both case the r.d.s. is the Volmer step (3); samples 10CV@NPG and 25CV@NPG pass respectively from 60 and 65 mV dec^{-1} to 73 and 78 mV dec^{-1}. For sample 5CV@NPG the slope decreases from 63 mV dec^{-1} to 31 mV dec^{-1} suggesting that the discharge reaction is the r.d.s. These results are promising considering the value of 71 mV dec^{-1} obtained for Pt. The present value is even better in comparison with 41 mV dec^{-1} of other MoS_2@NPGs [35], and lower than those of nanocrystalline MoS_2 (50-60 mV dec^{-1}) [44,41]. In Supporting Information **Table S2**, a comparison of electrochemical data with different MoS_2 and hybrid materials appeared in the literature is reported. In particular, the exchange current density decreases as a function of CV cycles, i.e. number of deposited layers, after the 10^{th} LSV cycles. A similar layer dependence has been reported for crystalline MoS_2 thin films growth on glassy carbon electrodes [45]. However, this trend is inverted when reaching 1000^{nd} cycles with an improvement of the exchange current density from 9 to 100 times with respect to the 10^{th} cycle. When the potential is swept during LSV the morphology of ligaments is changed: bare NPG shows an increased roughness (**Fig2b**), 5CV@NPG and 10CV@NPG ligaments show deposited MoS_2 aggregation of tens of nm while sample 25CV@NPG has a nano-grained layer covering the nanoporous structure. This redistribution of deposited material apparently enhances the performance of the electrode.

It is apparent also that the thickness of the MoS_2 layer is relevant since the best activity is found with sample 5CV@NPG having lower amount of deposited MoS_2. Actually, it has been demonstrated [40] that reduction of onset value and Tafel slope and increase of the exchange current density occur with monolayer MoS_2 with respect to multi-layers. A small amount, i.e. thickness, of deposited MoS_2 affords also to reduce the charge transfer resistance with a consequent faster electron transfer and high Faradaic efficiency during HER.

In summary, among the samples prepared, 5CV@NPG displays the best performance if compared with other samples described in this paper or in the literature. With an onset value of -31

mV, a Tafel slope of 31 mV/dec and an exchange current density of 0.09 μA cm^{-2} these sample is a good candidate as a catalyst for hydrogen evolution reaction in acidic environment.

Conclusions

In this paper NPG obtained by de-alloying an amorphous precursor has been electro-deposited by CV scan with amorphous MoS_2. Increasing the deposition time, i.e. number of CV cycles, ligaments are progressively encapsulated by a thin layer of MoS_2 until pores are partially occluded and a continuous film is formed on the surface. Sample preparation results faster and cheaper with respect to other techniques and also safer for the operator. Catalytic properties toward HER have been studied for MoS_2@NPG samples with open porosity during 1000 cycles, showing a general improvement: higher HER current density, lower onset of reaction compared with the literature and a Tafel slope in the range between 31 and 78 mV dec^{-1} depending on the sample. One of the samples, i.e. 5MoS_2@NPG, shows superior catalytic activity having an onset potential and a Tafel slope (-31 mV and 31 mV dec^{-1}) competitive with respect to Pt and other electrodes cited in the literature. Moreover mechanical stability, high surface area and high activity of bare NPG make MoS_2@NPG stable enough for real applications. The challenge to find ever a better catalyst of HER for large scale application is a balance between performance and costs. Even though this MoS_2@NPG samples could be considered as an expensive material due to the gold content approaching 16.5 karats, the reduced amount of ribbon needed for each electrode (about 10 mg/electrode) makes this solution economically sustainable compared with commercial Pt catalyst.

Acknowledgments

This work is supported by the European Commission, Marie Curie Actions — Initial Training Network (ITN), VitriMetTech — Vitrified Metals Technologies and Applications in Devices and Chemistry, 607080 FP7-PEOPLE-2013-ITN and also by BINGO Project–Torino call2014 L2 146 and Compagnia di SanPaolo.

References

[1] Poizot P, Dolhem F (2011) Clean energy new deal for a sustainable world: from non-CO_2 generating energy sources to greener electrochemical storage devices, Energy Environ. Sci. 4: 2003-2019.

[2] Rand DAJ, Dell RM (2007) Hydrogen Energy: Challenges and Prospects, RCS Publishing Cambridge.

[3] Turner JA (2004) Sustainable Hydrogen Production, Science 305:972-974.

[4] Hoffert M, Caldeira K et al. (2002) Engineering: Advanced technology paths to global climate stability: Energy for a greenhouse planet, Science 298:981-987.

[5] Ivy J (2004) Summary of electrolytic hydrogen production. Milestone completion report NREL/MP-560-36734. National Renewable Energy Laboratory: Golden, Colorado.

[6] Walter MG, Warren EL, McKone JR, Boettcher SW, Mi Q, Santori EA, Lewis NS (2010) Solar water splitting cells, Chem. Rev 110: 6446-6473.

[7] Bashyam R, Zelenay P (2006) A class of non-precious metal composite catalysts for fuel cells, Nature 443:63-66.

[8] Lu Q, Hutchings GS et al. (2015) Highly porous non-precious bimetallic electrocatalysts for efficient hydrogen evolution, Nature Communications 6:1-8.

[9] Hinnemann B, Moses PG, Bonde J, Jørgensen K P, Nielsen JH, Horch S, Chorkendorff I, Nørskovet JK (2005) Biomimetic Hydrogen Evolution: MoS2 Nanoparticles as Catalyst for Hydrogen Evolution J. Am. Chem. Soc. 127: 5308-5309.

[10] Lin C-H, Tsai C-H, Tseng F-G, Ma C-C M, Wu H-C, Hsieh C-K (2017) Three-dimensional vertically aligned hybrid nanoarchitecture of two-dimensional molybdenum disulfide nanosheets anchored on directly grown one-dimensional carbon nanotubes for use as a counter electrode in dye-sensitized solar cells, J Alloys and Comp. 692: 941-949.

[11] Recoraro TA, Chianelli RR (1981) J. Catal.67:430.

[12] Liu Y, Hu K, Hu E, Guo J, Han C, Hu X (2017) Double hollow MoS_2 nano-spheres: Synthesis, tribological properties, and functional conversion from lubrication to photocatalysis, Applied Surface Science 392:1144-1152.

[13] Topsøe H, Clausen BS, Massoth FE (1996) Hydrotreating Catalysis Science and Technology, vol. 11, edited by J. R. Anderson and M. Boudart, Springer, NewYork, NY,USA.

[14] Merki D, Fierro S, Vrubel H, Hu X (2011) Amorphous molybdenum sulfide films as catalysts for electrochemical hydrogen production in water, Chemical Science 2:1262-1267.

[15] Radisavljevic B, Radenovic A, Brivio J, Giacometti V, Kis A (2011) Single-Layer MoS_2 Transistors, Nat. Nanotechnol 6:147-150.

[16] Altavilla C, Sarno M, Ciambelli P (2011) A Novel Wet Chemistry Approach for the Synthesis of Hybrid 2D Free-Floating Single or Multilayer Nanosheets of MS_2@oleylamine(M=Mo, W), Chem. Mater. 23:3879-3885.

[17] Song I, Park C, Hong M, Baik J, Shin H-J, Choi H C (2014) Patternable Large-Scale Molybdenium Disulfide Atomic Layers Grown by Gold-Assisted Chemical Vapor Deposition, Angew. Chem. Int 53:1266-1269.

[18] Lauritsen JV, Kibsgaard J, Helveg S, Topsoe H, Clausen BS, Lagsgaard E, Besenbacher F (2007) Size-dependent structure of MoS_2 nanocrystals, Nat. Nanotechnol. 2:53-58.

[19] Peng Y, Meng Z, Zhong C, Lu J, Yu W, Jia Y, Qian Y (2001) Hydrothermal Synthesis and Characterization of Single-Molecular-Layer MoS_2 and $MoSe_2$, Chem. Lett. 30: 772-773.

[20] Fang M, Dong G, Wei R, Ho JC (2017) Hierarchical Nanostructures: Design for Sustainable Water Splitting, Adv. Energy Mater. *7*:1700559.

[21] Lee YH, Zhang XQ et al. (2012) Synthesis of large-area MoS2 atomic layers with chemical vapor deposition, Adv. Mater. 24:2320-2325.

[22] Morley TJ, Penner L, Schaffer P, Ruth TJ, Bénard F, Asselin E (2012) The deposition of smooth metallic molybdenum from aqueous electrolytes containing molybdate ions, Electrochemistry Communications, 15:78-80.

[23] Ghosh SK, Srivastava C, Nath S, Celis JP (2013) Simple Formation of Nanostructured Molybdenum Disulfide Thin Films by Electrodeposition, International Journal of Electrochemistry 1:1-7.

[24] Aliyevet AS, Elrouby M, Cafarova S F (2015) Electrochemical synthesis of molybdenum sulfide semiconductor, Materials Science in Semiconductor Processing 32:31-39.

[25] Lang X, Qian L, Guan P, Zi J, Chen MW (2011) Localized surface plasmon resonance of nanoporous gold, Appl. Phys. Letters 98:093701-3.

[26] Xue Y, Scaglione F, Rizzi P, Battezzati L (2017) Improving the chemical de-alloying of amorphous Au alloys, Corrosion Science 127:141-146.

[27] Zang L, Lang X, Hirata A, Chen MW (2011) Wrinkled Nanoporous Gold Films with Ultrahigh Surface-Enhanced Raman Scattering Enhancement, ACS Nano 6:4407-4413.

[28] Fang C, Shapter JG, Voelckerb NH, Ellis AV (2014) Electrochemically prepared nanoporous gold as a SERS substrate with high enhancement, RSC Adv. 4:19502-19506.

[29] Xu S, Yao Y, Wang P, Yang Y, Xia Y, Liu J, Li Z, Huang W (2013) Anodic Fabrication of Nanoporous Gold Films from Pure Gold in Oxalic Acid Solution and Their Applications in Electrocatalysis and SERS, Int. J. Electrochem. Sci. 8:1863-1870.

[30] Scaglione F, Celegato F, Rizzi P, Battezzati L (2015) A comparison of de-alloying crystalline and amorphous multicomponent Au alloys, Intermetallics 66:82-87.

[31] Van Petegem S, Brandstetter S, Maass R, Hodge AM, El-Dasher BS, Biener J, Schmitt B, Borca C, Swygenhoven H (2009) On the Microstructure of Nanoporous Gold: An X-ray Diffraction Study, Nano Lett. 9:1158-1163.

[32] Scaglione F, Rizzi P, Battezzati L (2012) De-alloying kinetics of an Au-based amorphous alloys, J Alloys and Comp. 536S:S60-S64.

[33] Rizzi P, Scaglione F, Battezzati L (2014) Nanoporous gold by dealloying of an amorphous precursor, J Alloys and Comp. 586:S117-S120.

[34] Paschalidou EM, Scaglione F, Gebert A, Oswald S, Rizzi P, Battezzati L (2016) Partially and fully de-alloyed glassy ribbons based on Au: Application in methanol electro-oxidation studies, J. Alloys and Compounds 667:302-309.

[35] Ge X, Chen L, Zhang L, Wen Y, Hirata A, Chen MW (2014) Nanoporous Metal Enhanced Catalytic Activities of Amorphous Molybdenum Sulfide for High-Efficiency Hydrogen Production, Adv. Mater. 26:3100-3104.

[36] Paschalidou EM, Celegato F, Scaglione F et al. (2016) The mechanism of generating nanoporous Au by de-alloying amorphous alloys, *Acta Materialia* 119:177-183.

[37] Ponomarev EA, Neumann-Spallart M, Hodes G, Levy-Clement C (1996) Electrochemical deposition of MoS_2 thin films by reduction of tetrathiomolybdate, *Thin Solid Films* 280:86-89.

[38] Nguyen DN, Nguyen LN, Nguyen PD, Thu T V, Nguyen AD, Tran PD (2016) Crystallization of Amorphous Molybdenum Sulfide Induced by Electron or Laser Beam and Its Effect on H_2-Evolving Activities, *J. Phys. Chem. C* 120:28789-28794.

[39] Murugesan S, Akkineni A, Chou BP, Glaz MS, Vanden Bout DA, Stevenson KJ (2013) Room Temperature Electrodeposition of Molybdenum Sulfide for Catalytic and Photoluminescence Applications, ACSNano 9:8199-8205.

[40] Tan Y, Liu P et al. (2014) Monolayer MoS_2 Films Supported by 3D Nanoporous Metals for High-Efficiency Electrocatalytic Hydrogen Production, Advanced Materials 26:8023-8028.

[41] Jaramillo TF, Jorgensen KP, Bonde J, Nielsen JH, Horch S, Chorkendorff I (2013) Identification of Active Edge Sites for Electrochemical H_2 Evolution from MoS_2 Nanocatalysts, Science 317:100-102.

[42] Bockris JOM, Potter CJ (1952) The Mechanism of the Cathodic Hydrogen Evolution Reaction, J. Electrochem. Soc. 99:169-186.

[43] Thomas JG (1961) Kinetics of Electrolytic Hyrdogen Evolution and the Adsorption of Hydrogen by Metals, Trans. Faraday Soc. 57:1603-1611.

[44] Kibsgaard Z, Chen B, Reinecke N, Jaramillo TF (2012) Engineering the surface structure of MoS_2 to preferentially expose active edge sites for electrocatalysis, Nat. Mater. 11:963-969.

[45] Yu Y, Huang S-Y, Li Y, S. Steinmann N, Yang W, Cao L (2014) Layer-Dependent Electrocatalysis of MoS_2 for Hydrogen Evolution, Nano Letters. 14:553-558.

Fig.1

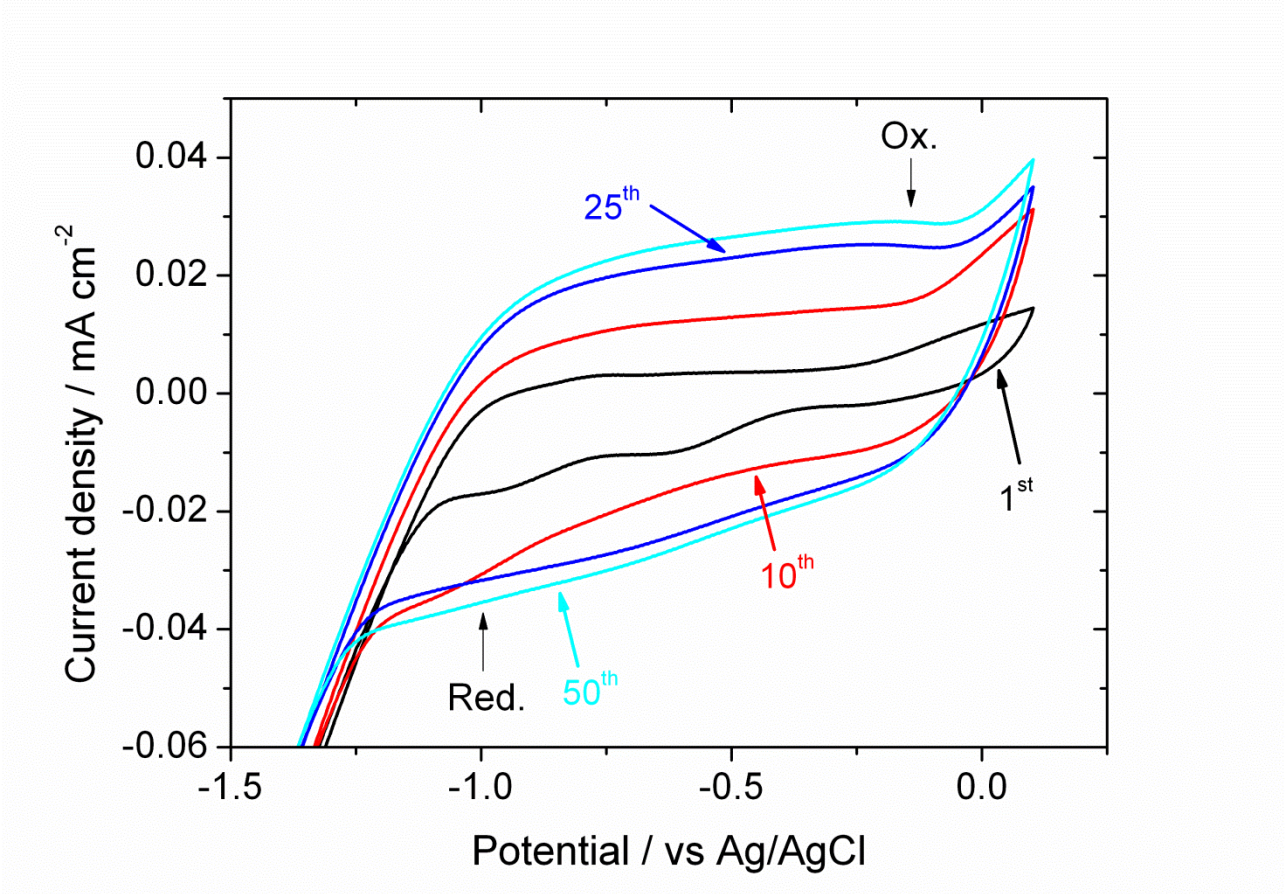

Fig.1. Electro-deposition of MoS_2 on NPG by repeated cyclic voltammetry (one up to 50 cycles) in a solution of 5mM $[MoS_4]^{-2}$ under mild stirring condition at room temperature.

Fig.2

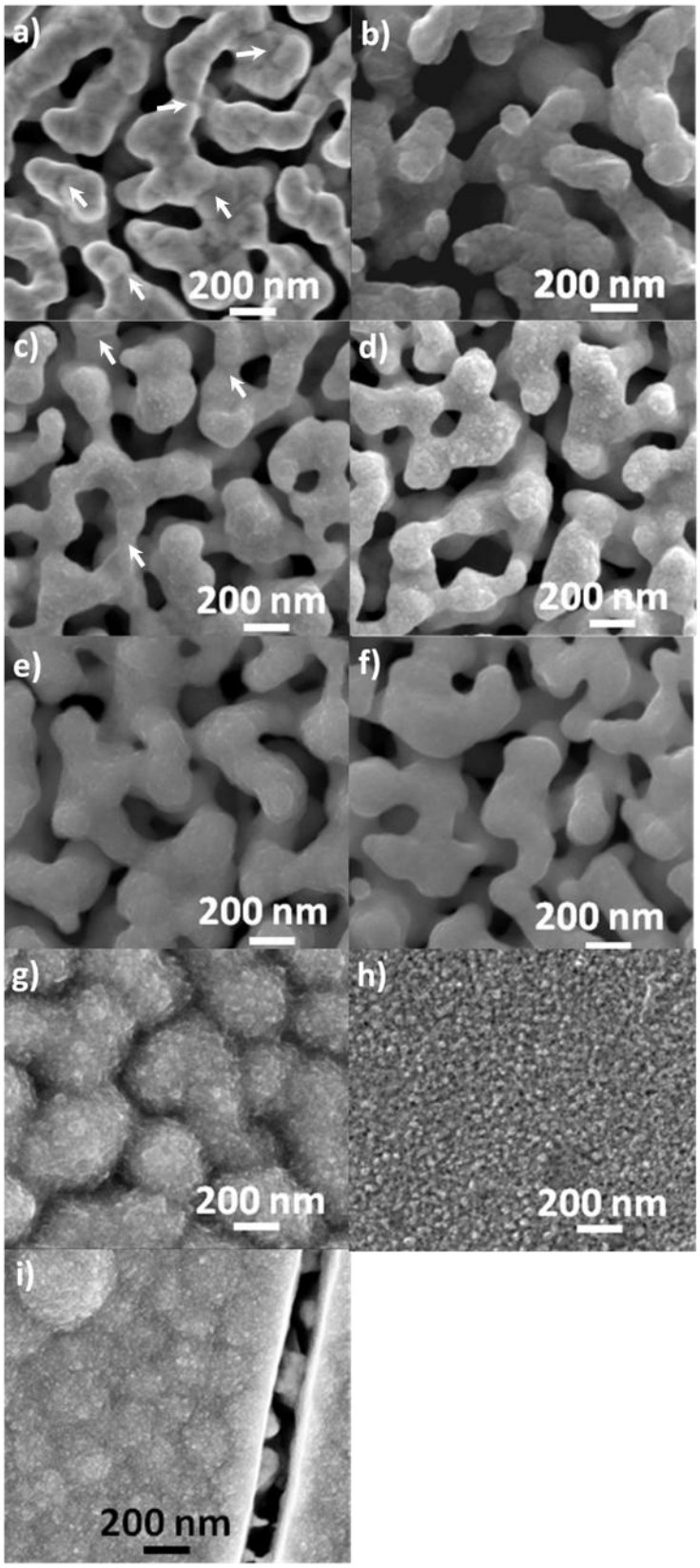
a)
200 nm
b)
200 nm
c)
200 nm
d)
200 nm
e)
200 nm
f)
200 nm
g)
200 nm
h)
200 nm
i)
200 nm

Fig.2. SEM images of samples before and after 1000 cycles of HER. a) and b) bare NPG, c) and d) 5CV@NPG, e) and f) 10CV@NPG, g) and h) 25CV@NPG, i) 50CV@NPG.

Fig.3

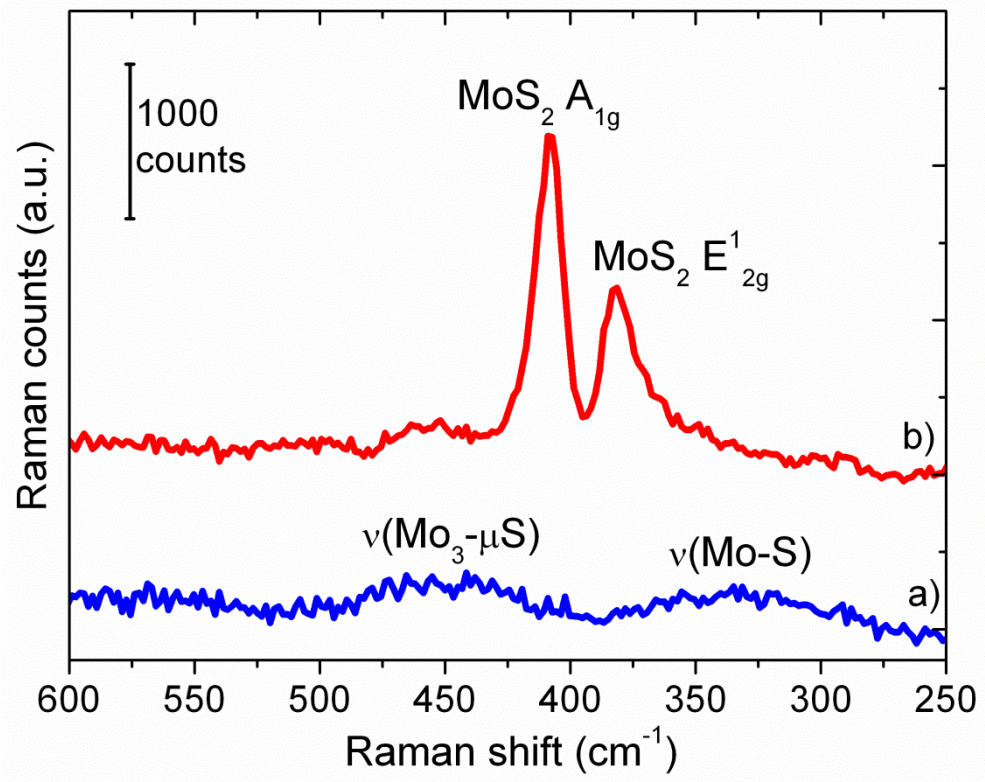

Fig.3. Raman analyses of a) the a-MoS_x deposited on NPG and b) the same sample after annealing to promote crystallization of c-MoS_2.

Fig.4

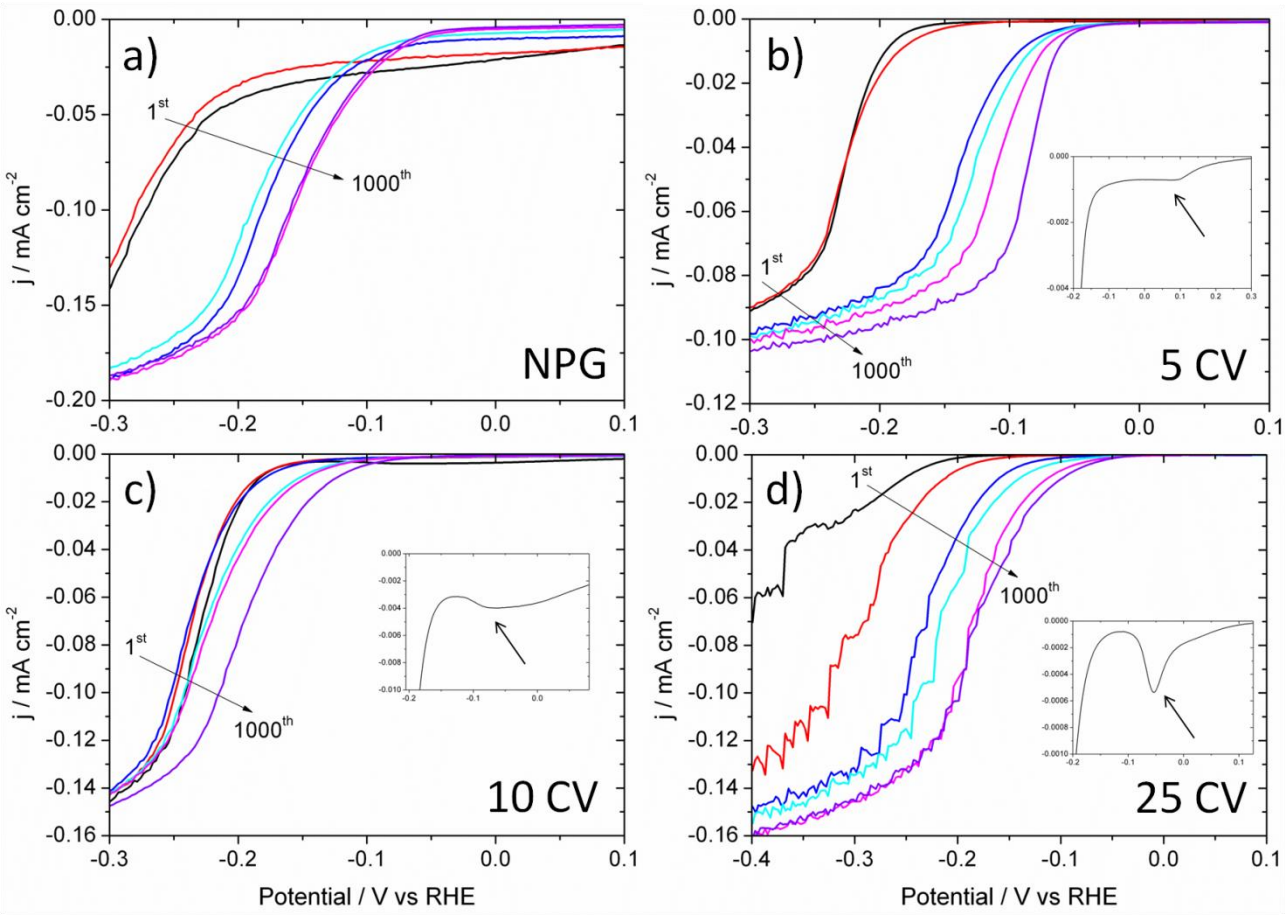

Fig.4. Polarization curves of a) bare NPG, and MoS_2@NPG after b) 5 CV, c) 10 CV and d) 25 CV; the insets show the reduction of MoS_3 to MoS_2 prior hydrogen evolution during the first cycle.

Fig.5

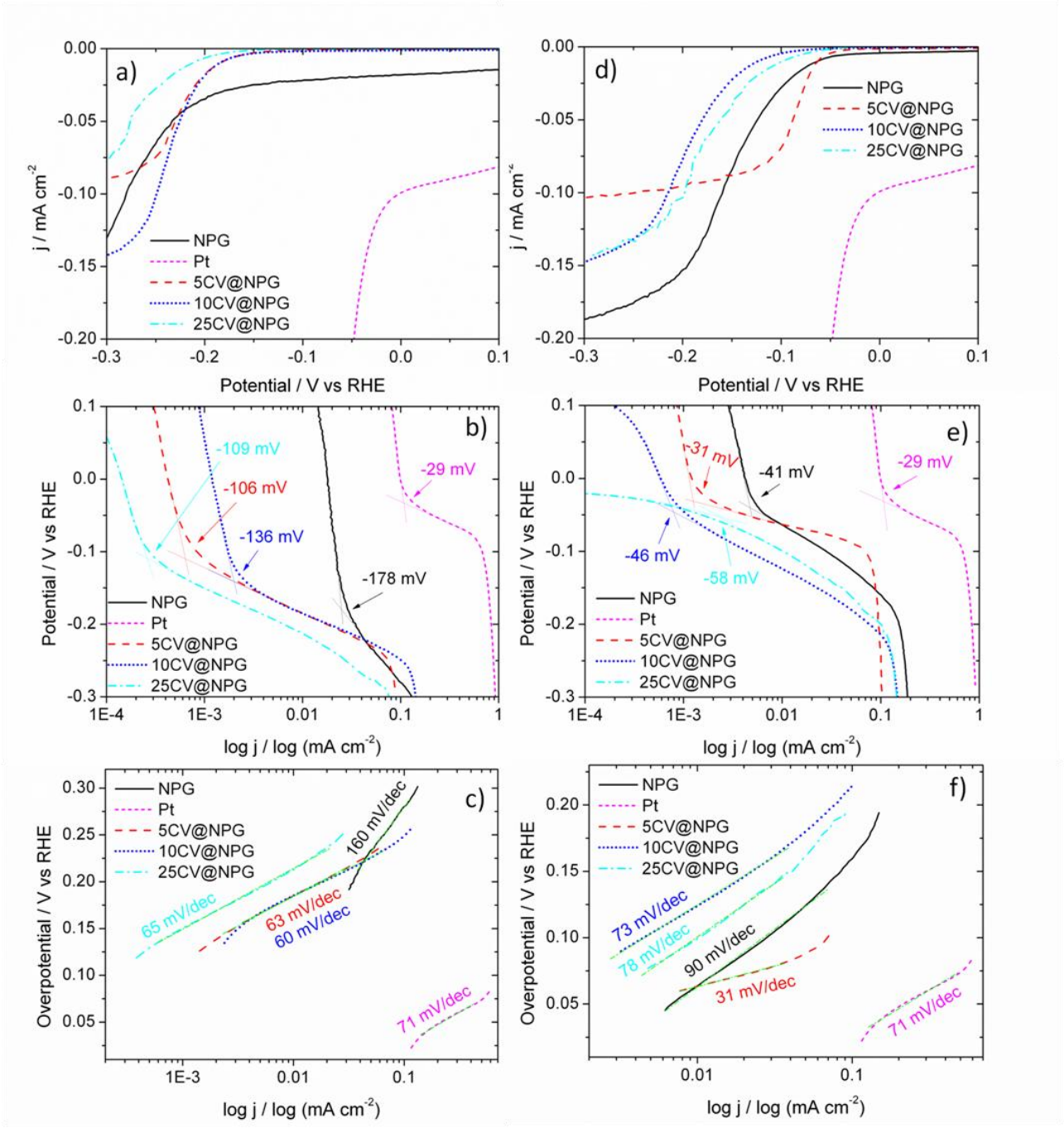

Fig.5. a) and d) HER polarization curves, b) and e) the onset HER potentials and c) and f) the Tafel plot of bare NPG and MoS_2@NPG after 5 CV, 10 CV and 25 CV; 10^{th} and 1000^{nd} cycles in 0.5 M H_2SO_4 @ RT respectively.